

CLIP-SR: Collaborative Linguistic and Image Processing for Super-Resolution

Bingwen Hu, Heng Liu, Zhedong Zheng, and Ping Liu, *Senior Member, IEEE*

Abstract—Convolutional Neural Networks (CNNs) have advanced Image Super-Resolution (SR), but most CNN-based methods rely solely on pixel-based transformations, often leading to artifacts and blurring, particularly with severe downsampling (e.g., $8\times$ or $16\times$). Recent text-guided SR methods attempt to leverage textual information for enhanced detail, but they frequently struggle with effective alignment, resulting in inconsistent semantic coherence. To address these limitations, we introduce a multi-modal semantic enhancement approach that combines textual semantics with visual features, effectively tackling semantic mismatches and detail loss in highly degraded LR images. Our proposed multi-modal collaborative framework enables the production of realistic and high-quality SR images at significant up-scaling factors. The framework integrates text and image inputs, employing a prompt predictor, Text-Image Fusion Block (TIFBlock), and Iterative Refinement Module alongside CLIP (Contrastive Language-Image Pretraining) features to guide a progressive enhancement process with fine-grained alignment. This alignment produces high-resolution outputs with crisp details and semantic coherence, even at large scaling factors. Through extensive comparative experiments and ablation studies, we validate the effectiveness of our approach. Additionally, by incorporating textual semantic guidance, our technique enables a degree of super-resolution editability while maintaining semantic coherence.

Index Terms—Image Super-Resolution, CLIP, Multi-modal Fusion, Language Guidance

I. INTRODUCTION

The advent of Convolutional Neural Networks (CNNs) has significantly advanced the field of image super-resolution (SR) [1]–[6]. Early CNN-based SR methods, which relied solely on low-resolution (LR) images to reconstruct high-resolution (HR) counterparts, often struggled to enhance reconstruction quality. To overcome these limitations, subsequent research [7]–[15] introduced prior information to guide the SR process, aiming to compensate for the missing details in LR images. While prior-based approaches have demonstrated improvements, they tend to be restricted to specific types of images, such as those with well-defined structures or attributes (e.g., facial images). Moreover, methods like SFTGAN [16], which leverage semantic segmentation maps to assist in SR reconstruction, often introduce additional computational costs and are highly dependent on the accuracy of the segmentation process.

To address these limitations, using text descriptions as a form of semantic guidance has emerged as a more flexible and comprehensive alternative. Text offers richer and more detailed semantic information, which can guide the super-resolution

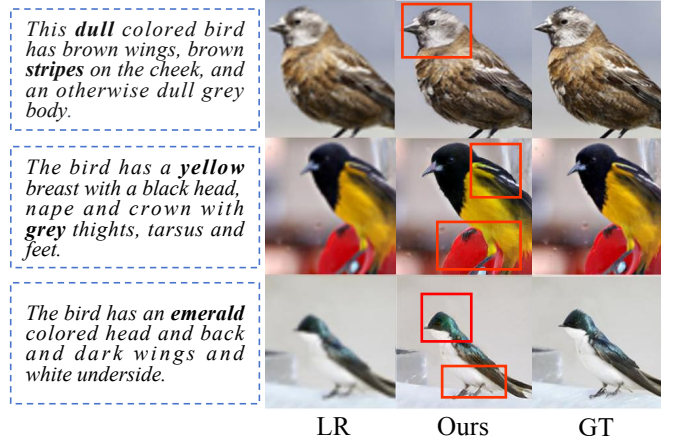


Fig. 1. Visualization results of our method to recover from the low-resolution inputs (LR). We highlight the semantic coherence part, by aligning with the textual guidance with the high-resolution (HR) ground truth.

process across a broader range of images. TGSR [17] was the first to explore this approach, using text to enhance SR image detail generation. However, challenges remain with this method, particularly in achieving effective text-image feature matching and semantic alignment, leading to inconsistencies between the input LR images and the generated SR results. In this paper, we propose a novel approach that ensures semantic consistency while achieving large-scale super-resolution. Our method leverages text descriptions to guide the SR process, ensuring that the reconstructed HR images are both semantically coherent and visually realistic. As shown in Figure 1, our approach addresses the limitations of previous methods, providing a robust solution for high-fidelity SR.

To address the challenges posed by the limitations of prior-based methods and ineffective text-image feature matching, particularly when dealing with large-scale resolution degradation and high semantic ambiguity in real-world scenarios, we introduce a novel approach: Multi-modal Collaborative Semantic Enhancement for Super-Resolution (SR). Rather than treating the relevant text as mere prior guidance, we leverage the text information in conjunction with the LR image as two modal inputs for SR tasks. Combining these modalities enhances local semantics and enables high-performance large-scale SR. Specifically, we introduce a prompt predictor designed to extract essential semantic elements from the text. Inspired by VPT [20] and GALIP [21], the prompt predictor incorporates a fully connected layer and a self-attention mechanism, serving as a text-driven attention module. Unlike directly inputting raw text vectors into the pre-trained CLIP-

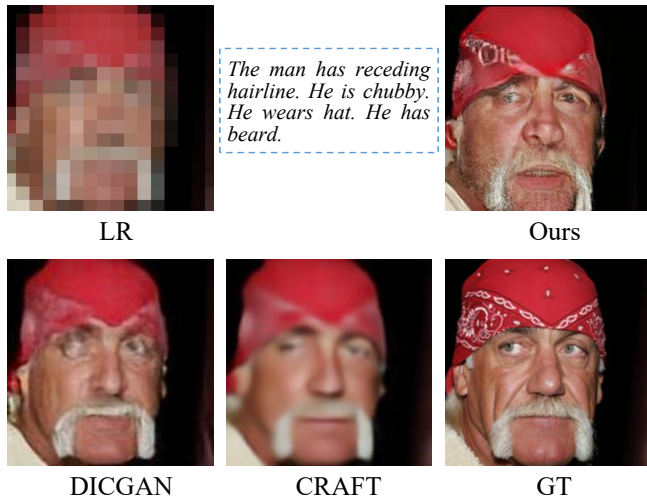


Fig. 2. An example $16\times$ image SR comparisons of ours and two SOTA SR methods: DICGAN [18] and CRAFT [19]. Here, DICGAN and CRAFT are re-trained with the same dataset as ours; LR is the input low-resolution image, and GT is the high-resolution ground truth (enlarged appropriately for visualization).

ViT, the refined text vectors generated by the prompt predictor enable CLIP-ViT to achieve enhanced alignment of semantic features between text and image, thereby improving the quality of cross-modal representation.

To further optimize text-image interactions, we introduce TIFBlock, a novel alignment fusion module specifically designed to enhance cross-modal integration. Leveraging pre-trained models like CLIP [22] for initial feature extraction, TIFBlock effectively synthesizes and refines these representations, resulting in a significant improvement in text-to-image matching performance. Building upon TIFBlock, we develop an iterative refinement module, a structure dedicated to iterative detail recovery and semantic enhancement. This module progressively refines local details, addressing blurred regions, while maintaining semantic consistency across iterations. A core component of the iterative refinement module is the inclusion of a customized residual connection tailored to our framework, which facilitates smooth feature propagation while preserving semantic integrity. The customized residual connection is seamlessly integrated within this module to further optimize pixel transition and feature propagation, ensuring robust multi-modal fusion. Together, these components align with our design objectives to deliver seamless and effective collaboration between modalities.

By effectively incorporating textual descriptions associated with the given LR image in a language-informed manner, the proposed method generates highly detailed SR results. As illustrated in Figure 2, we showcase a typical example of our method applied to a severely downsampled face image with a $16\times$ SR factor. Our approach demonstrates competitive performance when compared to two state-of-the-art SR methods. Additionally, the proposed method exhibits strong interpretability and semantic consistency with the provided text descriptions.

The primary contributions of this work are as follows:

- We introduce a new multi-modal semantic coherence

approach for large-scale image super-resolution, generating semantically consistent and realistic high-resolution images from severely degraded low-resolution inputs.

- We design a novel Text-Image Fusion Block (TIFBlock) and integrate it with a pre-trained cross-modality model to create an iterative collaborative fusion structure, making our framework progressively restore image details while enhancing local semantics.
- We investigate the impact of diverse textual semantics on the image super-resolution. Comprehensive comparative experiments and ablation studies validate the effectiveness of our SR approach while maintaining semantic coherence.

II. RELATED WORK

A. Prior-based Image Super-Resolution

Single Image Super-Resolution (SR) has become a dynamic area within end-to-end deep learning [23]. The development of diverse models and mechanisms has significantly improved SR methods, particularly in pixel reconstruction and detail approximation. Early SR approaches [4], [24]–[28], usually assume the LR image pixels are obtained through bicubic down-sampling on HR counterparts. These methods employ various deep mapping networks to directly reconstruct SR image pixels from LR inputs. While these approaches can achieve promising results on synthetic data with small-scale degradation, their effectiveness will deteriorate significantly in real-world large-scale degradation scenarios due to the full or partial loss of LR semantics.

To improve performance in real-world SR scenarios, numerous prior-based approaches have been proposed, deploying explicit or implicit priors to enrich detail generation. A representative explicit method is reference-based SR [29]–[32], which leverages one or more high-resolution reference images that share similar textures with the input low-resolution image to guide the generation of the HR output. However, matching features of the reference with low-resolution input could be challenging, and these explicit priors may not be available.

Recent methods, including FSRNet [7], DeepSEE [11], SFTGAN [8], TGSR [17], have shifted toward leveraging implicit priors, achieving improved results by integrating prior information directly into the SR process. For instance, FSRNet [7] leverages geometric priors to improve face image SR effects, while Zhang *et al.* [33] harnesses the multi-view consistency. DeepSEE [11] utilizes semantic maps to explore extreme image SR. SFTGAN [8] introduces image segmentation masks as prior features for face image SR, and TGSR [17] employs text semantics as a prior condition to guide image SR. Although effective, these implicit priors are often tailored to specific situations, such as restricted categories [34], [35], or facial images [7], [8], [36], [37], limiting their applicability to more complex, real-world SR tasks.

B. Multi-modal Fusion Guided Image Generation

Multi-modal fusion has become increasingly prevalent in various visual tasks, such as image generation, style transfer, and image editing. For example, keypoints are commonly

utilized in motion generation [38] and automatic makeup applications [39]. In text-based image synthesis, GAN-INTCLS [40] employs text descriptions to generate images using conditional Generative Adversarial Networks (cGANs). To enhance image quality, Stack-GAN [41], AttnGAN [42], and DM-GAN [43] leverage multiple generators and discriminators. DF-GAN [44] simplifies text-to-image synthesis with a more streamlined and effective approach. LAFITE [45] introduces a contrastive loss based on the CLIP model [22], offering more accurate guidance for generating precise images. In artistic style transfer, CLIPstyler [46] enables domain-independent texture transfer from text descriptions to source images, while CLVA [47] employs a patch-wise style discriminator to extract visual semantics from style instructions, achieving detailed and localized artistic style transfer. For text-guided image editing, SISGAN [48] pioneers methods using an encoder-decoder architecture for text-based semantic editing. ManiGAN [49] introduces a two-stage architecture with ACM (attentional crop module) and DCM (deformable crop module) to facilitate independent network training for text-based image editing. Lightweight GAN [40] further improves efficiency by applying a word-level discriminator. ManiTrans [50] employs a pre-trained auto-regressive transformer, utilizing the CLIP model [22] for semantic loss. More recently, Zeng *et al.* [51] develops a multi-round image editing framework using language guidance.

The emergence of large-language models has further spurred advancements in text-to-image generation. DALL-E [52] uses VQ-VAE [53] to decompose images into discrete tokens, framing image synthesis as a translation task. LDM [54] applies diffusion models to latent image vectors, allowing efficient training with high-quality results. GLIDE [55], a diffusion-based text-to-image generation model, uses guided diffusion to enhance text-conditioned synthesis. GALIP [21] incorporates the CLIP model within adversarial learning for text-to-image synthesis. ControlNet [56], introduced by Zhang *et al.*, builds upon the pre-trained Stable Diffusion [54], incorporating detailed control to guide image generation.

Recent advancements in pre-trained diffusion models [54], [55], [57] have significantly improved image generation capabilities. While studies [58]–[62] underscore the generative potential of these models, their application to SR remains challenging. The high fidelity required for SR demands both speed and efficiency—qualities that diffusion models generally lack due to their multi-step denoising process, which results in slower generation times and complicates latent space manipulation.

Compared to using diffusion models, this work employs a GAN-based model for several key reasons. GANs facilitate high-resolution image generation in a single pass, which significantly enhances efficiency compared to the iterative nature of diffusion models. Furthermore, they provide a smooth latent space that enables intuitive control over generated features, making them particularly well-suited for SR tasks. Additionally, GANs require less training data and computational resources, improving accessibility for researchers. By leveraging GANs, we aim to achieve high-quality image generation while ensuring the practical applicability of super-resolution.

III. METHOD

In this section, we present an overview of our proposed CLIP-SR, followed by detailed descriptions of each component within our multi-modal cooperative image super-resolution (SR) network. Finally, we introduce the total loss function used in our approach.

A. Overview

Traditional small-factor SR methods generate HR images from LR images using deep SR networks. However, large-factor downsampling often leads to significant blurring of LR images, making it challenging for SR networks to reconstruct semantically consistent and precise details solely from pixel-space information. To address these challenges, we introduce textual semantics as a complementary input, enabling our network to leverage information from both pixel and textual spaces for more accurate detail generation. Clearly, we denote the input low-resolution image as L_{LR} , the complementary text description as T , and the high-resolution ground truth as I_{GT} , corresponding to the input low-resolution image L_{LR} . The objective of CLIP-SR \mathcal{H} is to fuse L_{LR} and T to generate a semantically consistent and visually realistic super-resolution image, denoted as I_{SR} .

Specifically, we introduce a text-image fusion block (TIF-Block) within a multi-modal iterative refinement model, which integrates CLIP [22] and TIFBlock to achieve effective large-factor SR. To efficiently combine information from different modalities, *i.e.*, text, and image, we design a robust fusion strategy that preserves essential textual details while avoiding the information loss observed in simpler approaches [41], [48], [63] that directly merge text vectors with image features. Our TIFBlock employs an affine transformation alignment strategy to enhance fusion text-image accuracy and retain critical semantic details. Given the inherent differences between text and image features, precise alignment is crucial for achieving semantic coherence. To further reduce cross-modal inconsistencies, a prompt predictor is employed to process the text vectors prior to alignment. Additionally, the CLIP model [22] is integrated within our framework as a supplementary alignment tool, ensuring contextually precise and semantically coherent text-image fusion for SR.

To further ensure coherence with the LR content in the generated SR image, we design two additional mechanisms that build on our fusion strategy. Specifically, we incorporate residual connections to preserve essential LR details, particularly in cases where semantic conflicts may arise. Additionally, text semantics are integrated at each layer of the multi-modal iterative refinement module, progressively guiding the SR process with fine-grained adjustments. Those refined semantic fusion strategies ensure that the generated SR image remains both structurally and semantically consistent with the LR input. Figure 3 provides an overview of the overall network architecture and details of the designed TIFBlock.

B. Network Architecture

In this section, we present the key components of our proposed multi-modal large-factor image super-resolution model.

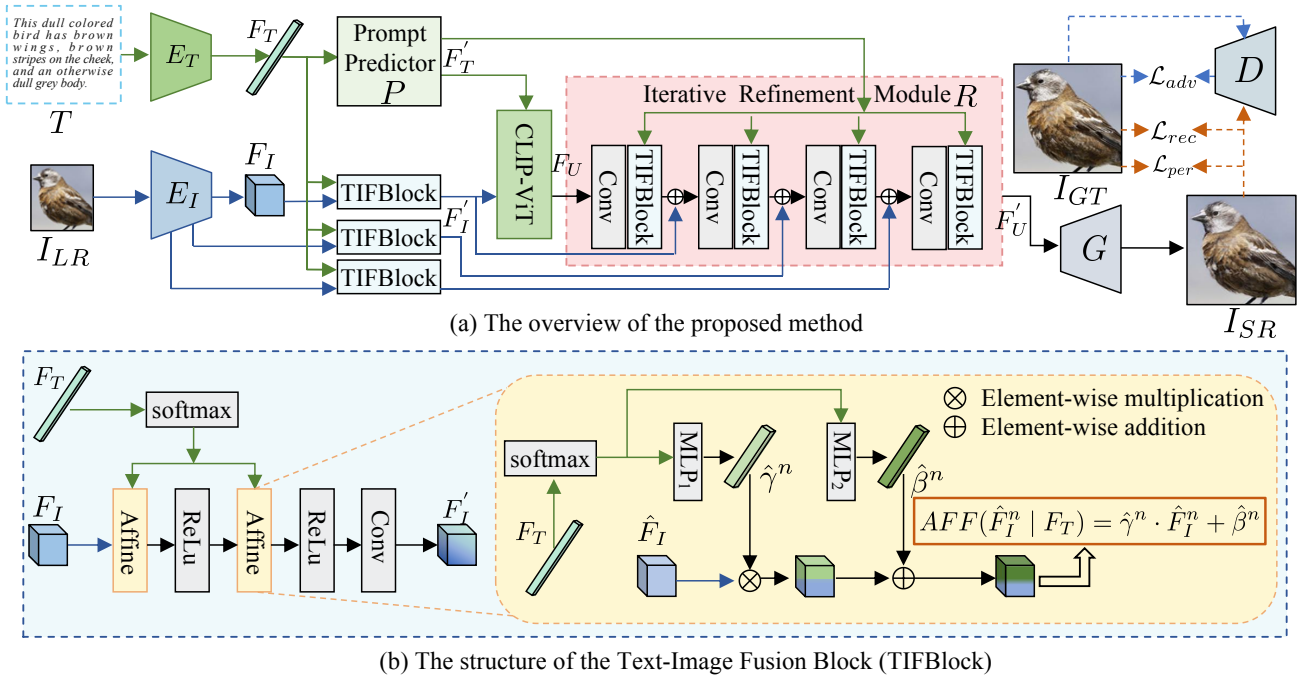


Fig. 3. The architecture of our proposed multi-modal cooperative semantic enhancement model for large-factor image super-resolution (see subfigure (a)). Given an input low-resolution image I_{LR} and text guidance T , features F_I and F_T are first extracted using an image encoder E_I and a text encoder E_T , respectively. The text feature vector F_T is further refined through a prompt predictor module P and then processed by the CLIP-ViT model to enhance textual guidance. Subsequently, the refined text and image features are integrated using a Text-Image Fusion Block (TIFBlock), which aligns and combines the two modalities (see subfigure (b)). Within the TIFBlock, an affine transformation is applied in its text fusion module. This transformation employs two consecutive Multi-Layer Perceptrons (MLPs) to generate channel-wise scaling parameters ($\hat{\gamma}^n = MLP_1(\text{Softmax}(F_T))$) and shifting parameters ($\hat{\beta}^n = MLP_2(\text{Softmax}(F_T))$). These parameters adaptively modulate the channel-wise features of the visual representation F_I^n . Finally, the fused multi-modal features undergo iterative refinement and semantic enhancement through a continuous Conv-TIFBlock structure, referred to as the iterative refinement module R . This iterative process ensures progressively improved super-resolution outputs with enhanced details and semantic coherence.

The model primarily comprises five components: text and image encoders, the prompt predictor, the text-image fusion block (TIFBlock), the iterative refinement module, and the CLIP-based discriminator.

In essence, the text and image encoders extract text vectors and image features, providing foundational representations for the following steps. The TIFBlock aligns and fuses these features, enabling cohesive integration of textual and visual information. The CLIP-ViT and the prompt predictor effectively enhance textual guidance throughout the generation process. The iterative refinement module progressively restores image details and enhances local semantics through multiple iterations, ensuring the alignment between different modalities. Finally, the CLIP-based discriminator comprehensively evaluates the fidelity, semantic quality, and coherence of the generated image. By leveraging the synergistic interaction of these five components, our method generates semantically consistent and realistically reconstructed high-resolution images, even from severely degraded low-resolution inputs (e.g., $8\times$ or $16\times$ downsampling).

1) *Text and Image Encoders*: We utilize two distinct encoders to process the input modalities. The text encoder, denoted as E_T , follows the architecture of CLIP [22] and encodes textual inputs T into feature vectors F_T , where $F_T = E_T(T)$, to effectively capture semantic information. For input LR images I_{LR} , the image encoder E_I employs a series of convolutional layers to progressively transform the

input into an 8×8 feature map F_I , where $F_I = E_I(I_{LR})$. These encoders allow our model to generate compatible feature representations for both text and image inputs, preparing them for following fusion within the network.

2) *Prompt Predictor*: Before leveraging the pre-trained CLIP-ViT to align image features with corresponding text vectors, we introduce a prompt predictor inspired by VPT [20] and GALIP [21]. The prompt predictor, denoted as P , comprises a fully connected (FC) layer and a self-attention layer, functioning as a text-driven attention mechanism. It predicts text-conditioned prompts, $F'_T = P(F_T)$, which are appended to the visual patch embeddings in CLIP-ViT. This design enables the generated images to more effectively capture the semantic content of the input text while maintaining alignment with the visual information encoded by the CLIP-ViT model.

The prompt predictor leverages the output of the text encoder to selectively focus on salient textual elements, which are then fused with the visual features. This integration enables the generator to more accurately interpret and translate the text into detailed, coherent visual representations, enhancing alignment between text descriptions and the generated images in both content and quality.

3) *Text-Image Fusion Block (TIFBlock)*: To further enhance the influence of text information on images, we introduce a Text-Image Fusion Block (TIFBlock) that integrates textual semantics as a complementary feature source. As shown in Figure 3 (b), TIFBlock incorporates an affine transformation

within its text fusion module. Following the design principles from DF-GAN [44], we introduce a ReLU layer after each affine layer to increase the diversity of text-fused images by introducing non-linear relationships. Additionally, to improve the model’s comprehension of text descriptions, we apply a Softmax function to re-weight the text features before passing them into the affine layer. This re-weighting strategy allows for smoother and more reliable integration of text and image domains.

The process of TIFBlock starts by feeding the LR image I_{LR} into the image encoder network E_I , extracting the image feature F_I . Meanwhile, the text is encoded via the pre-trained CLIP encoder E_T , producing the text vector F_T . The text features are then re-weighted using the Softmax function before being passed through the affine transformation layer. Within this layer, the re-weighted text vector is processed through two consecutive Multi-Layer Perceptrons (MLPs), which generate the channel-wise scaling parameter $\hat{\gamma} = MLP_1(\text{Softmax}(F_T))$ and the channel-wise shifting parameter $\hat{\beta} = MLP_2(\text{Softmax}(F_T))$. The affine transformation then adaptively adjusts the channel-wise features of the visual feature \hat{F}_I^n . The affine transformation is defined as follows:

$$AFF(\hat{F}_I^n | F_T) = \hat{\gamma}^n \cdot \hat{F}_I^n + \hat{\beta}^n, \quad (1)$$

where AFF denotes the affine transformation, \hat{F}_I^n represents the n -th channel of the visual feature map \hat{F}_I , F_T represents the text vector, and $\hat{\gamma}^n$ and $\hat{\beta}^n$ are learnable scaling and shifting parameters. This mechanism enables the model to dynamically adjust the feature response to the textual context, leading to more accurate and meaningful alignment.

The TIFBlock performs the initial alignment and integration of text and image features by fusing the modalities through affine transformations, ensuring semantic consistency and accurate feature combination. These fused multi-modal features are then passed into the Iterative Refinement Module, which progressively enhances the image quality by refining local details and reinforcing semantic coherence through multiple iterations. The iterative process builds on the fused features provided by the TIFBlock, enabling the model to generate outputs with higher resolution and realistic textures. Together, the TIFBlock establishes the foundational alignment of modalities, while the Iterative Refinement Module further optimizes and restores the image details step by step.

4) *Iterative Refinement Module*: To ensure the generated image aligns closely with the given text, we iteratively refine the image features derived from CLIP-ViT, using a residual structure to fuse text-image features guided by the text vector. Initially, the prompt predictor leverages the output of the text encoder to bridge the semantic gap between text and image modalities. Subsequently, the low-resolution image features F_I are combined with the text vector F_T within the TIFBlock to further align the image and text features. CLIP-ViT is then employed to reconcile any inconsistencies between the image and text, ensuring that the final image features match the knowledge existing in both modalities. Finally, the outputs from the prompt predictor, TIFBlock, and CLIP-ViT are iteratively merged via the residual structure to generate a

high-resolution image that is semantically consistent with the provided text.

Throughout the entire pipeline, we utilize text information at three key stages. First, we employ a simple convolutional network to extract features from the low-resolution image, which are integrated with text information using the TIFBlock. This integration ensures that the combined features encapsulate both detailed visual cues and semantic information, enabling precise guidance of the information flow within the CLIP-ViT network. Next, a text attention mechanism processes the textual features to address the inherent differences between text and image modalities, facilitating effective cross-modal alignment. Additionally, the textual information serves as input to a prompt predictor that feeds into the CLIP-ViT model, further enhancing the fusion of visual and semantic features. Finally, after obtaining preliminary image features from the CLIP-ViT, the iterative refinement module progressively restores detailed image information by iteratively fusing it with textual semantics and enlarging the image through an additional upsampling module G .

5) *CLIP-based Discriminator*: We utilize the CLIP-based discriminator proposed by GALIP [21], which extracts more informative visual features from complex images, enabling the discriminator to more effectively identify unrealistic image regions. This, in turn, prompts the generator to produce more realistic images. The structure of the discriminator demonstrates a deep understanding of complex scenes by integrating additional visual information into the CLIP framework, making it particularly well-suited for its role as a discriminator. Specifically, the CLIP-based discriminator is designed to incorporate the language-image pre-training of CLIP [22], with enhancements tailored to improve its effectiveness in evaluating the quality of generated images.

During training, the discriminator aims to distinguish between generated and real images. The CLIP model’s superior performance in aligning text and images from different modalities allows the CLIP-based discriminator to gain a comprehensive and nuanced understanding of the image content, contributing to the generation of higher-quality and semantically consistent outputs in our proposed method.

C. Optimization Objectives

Reconstruction Loss. To ensure consistency in the content of reconstructed images, we employ the pixel-wise \mathcal{L}_1 -norm, defined as follows:

$$\mathcal{L}_{rec} = \mathbb{E}[\|\mathcal{H}(I_{LR}, T) - I_{GT}\|_1], \quad (2)$$

where $\mathcal{H}(I_{LR}, T)$ denotes the output generated by the full super-resolution network \mathcal{H} proposed in this work, F_T represents the text description, and I_{GT} represents the high-resolution ground truth corresponding to the input low-resolution image I_{LR} .

Perceptual Loss. Additionally, we use the perceptual loss [64] to encourage visual consistency between the generated

TABLE I
THE DATASET STATISTICS. TEXT/IMAGE REPRESENTS THE NUMBER OF WORDS CORRESPONDING TO EACH IMAGE.

Dataset	CUB		CelebA		COCO	
	train	test	train	test	train	test
Images	8,855	2,933	24,000	6,000	82,783	40,470
Text/Image	10	10	10	10	5	5

super-resolution results and the real high-resolution images. The perceptual loss is defined as follows:

$$\mathcal{L}_{per} = \mathbb{E} \left[\sum_{i=0}^5 \sigma_i \|\phi_i(\mathcal{H}(I_{LR}, T)) - \phi_i(I_{GT})\|_1 \right], \quad (3)$$

where $\phi_i(\cdot)$ denotes the feature map from the i -th layer of the pre-trained perception network ϕ . We employ the pre-trained VGG-19 network [65] as our ϕ and select five activation layers to compute the perceptual loss. The hyper-parameters σ_i modulate the contribution of the i -th layer to the total loss term in Equation 3.

Text-Constrained Adversarial Loss. To constrain the semantic information of the text, we utilize the text-constrained adversarial loss [21]. Here, I_{LR} represents a given low-resolution image, and F_T is the text vector extracted from the corresponding text input. Both the low-resolution image I_{LR} and the text vector F_T are fed into the super-resolution network \mathcal{H} , resulting in the output $\mathcal{H}(I_{LR}, T)$. Let \mathcal{C} and \mathcal{V} represent the frozen CLIP-ViT model and the image feature extractor model in the CLIP-based discriminator. $Sim(\cdot, \cdot)$ denotes the cosine similarity between the generated HR image $\mathcal{H}(I_{LR}, F_T)$ and the text vector F_T .

The text-constrained adversarial loss is defined as follows:

$$\begin{aligned} \mathcal{L}_{adv} = & -\mathbb{E}_{(\mathcal{H}(I_{LR}, T) \sim \mathbb{P}_g)} [D(\mathcal{C}(\mathcal{H}(I_{LR}, T), F_T))] \\ & - \alpha \mathbb{E}_{(\mathcal{H}(I_{LR}, T) \sim \mathbb{P}_g)} [Sim(\mathcal{V}(\mathcal{H}(I_{LR}, T)), F_T)], \end{aligned} \quad (4)$$

where α is a hyper-parameter that controls the weight of the text-image similarity, and \mathbb{P}_g denotes the synthetic data distribution.

Total Loss. Taking all of the above loss functions into account, the total objective function is formulated as follows:

$$\mathcal{L}_{total} = \mathcal{L}_{rec} + \mathcal{L}_{per} + \lambda_{adv} \mathcal{L}_{adv}, \quad (5)$$

where the hyper-parameter λ_{adv} controls the weight of the adversarial loss \mathcal{L}_{adv} .

IV. EXPERIMENT

A. Implementation Details

Dataset. We evaluate our method on the COCO [66], Birds200 (CUB) [67], and CelebA [68] datasets, each containing images paired with textual descriptions as summarized in Table I. For training, all images are cropped to 256×256 resolution, with low-resolution images generated via Bicubic downsampling of high-resolution counterparts. The CLIP-ViT backbone used is the ViT-B/32 model.

Setting. We train the proposed method on an NVIDIA RTX A5000, using the Adam optimizer with parameters $\beta_1 = 0.0$

and $\beta_2 = 0.9$ over 220 epochs. The hyper-parameter λ_{adv} is set to 0.01. Meanwhile, following the setup in GALIP [21], we set α to 4. Since the official code for TGSR [17] is unavailable, we denote TGSR[#] to represent results reproduced based on the visual examples and quantitative metrics provided in the TGSR paper for comparison with other methods.

B. Quantitative Evaluation

To quantitatively assess the quality of the SR images generated by different methods, we utilize two primary evaluation metrics: NIQE (Natural Image Quality Evaluator) [69] and PI (Perceptual Index) [70]. NIQE evaluates the overall quality of SR images, with lower scores indicating more natural and realistic results. PI, on the other hand, measures the perceptual quality of the images, where lower PI values correspond to better visual quality. We specifically choose NIQE and PI for our experiments (except for Table III) instead of traditional metrics like PSNR and SSIM, which focus more on image distortion but overlook objective quality and perceptual experience. In the context of super-resolution, NIQE and PI are more aligned with assessing the realism and naturalness of images, making them better suited for this task.

Table II presents our experimental results on the CUB and COCO datasets. For the smaller CUB dataset, we compare NIQE and PI scores against several state-of-the-art super-resolution methods, including EDSR [1], ESRGAN [2], SPSR [12], and TGSR[#] [17]. Our method achieves the second-best NIQE score, closely following ESRGAN, while outperforming both Bicubic interpolation and EDSR in terms of PI. On the larger COCO dataset, our approach significantly outperforms all comparison methods in both NIQE and PI, demonstrating superior generalization capability. The observed performance degradation of other approaches on COCO further underscores the robustness and versatility of our method.

Table III provides a quantitative comparison of PSNR, SSIM, NIQE, and PI metrics on the CelebA dataset. Our method is evaluated against several baseline approaches, including Bicubic interpolation, SuperFAN [9], DICGAN [18], and TGSR[#] [17]. The results demonstrate that the proposed method achieves competitive performance across all metrics. Specifically, compared to Bicubic interpolation, SuperFAN, and DICGAN, which rely solely on single-modality input, our approach incorporates supplementary textual information to achieve cross-modal semantic alignment, resulting in superior super-resolution performance. Moreover, in comparison to TGSR[#], which also utilizes text guidance, our multi-modal collaborative semantic enhancement mechanism produces high-resolution images that are both semantically consistent and visually realistic. In summary, our method consistently delivers competitive results across three datasets, underscoring its effectiveness in image super-resolution tasks.

C. Qualitative Evaluation

To validate the effectiveness of the proposed method further, we conduct additional qualitative experiments. Specifically, we replace the pre-trained CLIP-ViT model in our original framework with BLIP-2 [71] substituting the text encoder

TABLE II

QUANTITATIVE COMPARISON OF OUR METHOD AND THE COMPARATIVE METHODS ON THE CUB AND COCO DATASETS. THE SYMBOL \downarrow DENOTES THAT THE LOWER METRIC IS BETTER.

Dataset	Metrics	Bicubic	EDSR [1]	ESRGAN [2]	SPSR [12]	TGSR# [17]	Ours
CUB	NIQE \downarrow	12.374	10.684	5.465	5.885	6.623	5.825
	PI \downarrow	9.747	8.168	2.644	3.345	2.560	4.167
COCO	NIQE \downarrow	11.110	9.683	6.816	6.378	6.484	4.706
	PI \downarrow	9.373	8.515	7.135	6.060	4.922	3.610

TABLE III

QUANTITATIVE COMPARISONS ON THE CELEBA DATASETS.

Metrics	Bicubic	SuperFAN [9]	DICGAN [18]	TGSR# [17]	Ours
PSNR \uparrow	25.81	28.908	33.61	23.48	28.974
SSIM \uparrow	0.844	0.815	0.895	0.766	0.808
NIQE \downarrow	14.514	6.459	5.755	8.846	5.172
PI \downarrow	9.676	5.345	5.5986	7.165	4.476

from CLIP to BERT [72]. We then retrained the network on the CUB dataset, denoting the visual results obtained after retraining as *Ours**. As illustrated in Figure 4, the experimental results demonstrate that our method achieves satisfactory visual outcomes even with this modification. These findings further confirm that the proposed multi-modal collaborative framework can consistently generate high-quality SR images with clear details and strong semantic coherence.

Concurrently, we perform an additional super-resolution (SR) experiment that upscales the low-resolution images from 64×64 to 256×256 . As illustrated in Figure 5, our method, along with the comparison methods SuperFAN [9] and DICGAN [18], generates SR images with commendable visual quality. However, the outputs from SuperFAN and DICGAN exhibit noticeable artifacts, while our method produces significantly smoother and more visually appealing results. These findings demonstrate that our approach outperforms single-modal methods in SR tasks by leveraging supplementary textual information to achieve effective cross-modal semantic alignment.

Additionally, Figure 6 presents qualitative results for $16 \times$ super-resolution on the CelebA dataset. The visualizations show that CRAFT [19] often produces overly smoothed images, limiting its ability to recover fine details. In contrast, our method achieves super-resolution at 256×256 , demonstrating its ability to meet two primary objectives: (1) restoring a substantial portion of the original image’s semantic information, and (2) maintaining high consistency between the SR output and the original low-resolution input.

D. Ablation Studies and Further Discussion

To evaluate the effectiveness of each component in our proposed method, we conducted ablation studies on the CUB dataset. We consider four variants: (1) a baseline U-Net for single image super-resolution, where $\mathcal{L}_{total} = \mathcal{L}_{rec} + \mathcal{L}_{per}$; (2) variant 1 with additional text supervision, incorporating our proposed multi-modal fusion architecture (TIFBlock and iterative refinement module), where $\mathcal{L}_{total} = \mathcal{L}_{rec} + \mathcal{L}_{per}$;

TABLE IV

COMPARISON OF QUANTITATIVE RESULTS OF DIFFERENT COMPONENTS OF OUR METHOD ON THE CUB DATASET.

Variants	U-Net	Text	CLIP-ViT	\mathcal{L}_{adv}	NIQE \downarrow
1	✓	✗	✗	✗	7.920
2	✓	✓	✗	✗	7.905
3	✓	✓	✓	✗	7.831
4	✓	✓	✗	✓	6.336
Ours	✓	✓	✓	✓	5.825

(3) variant 2 with a pre-trained CLIP-ViT model, where $\mathcal{L}_{total} = \mathcal{L}_{rec} + \mathcal{L}_{per}$; and (4) variant 2 with a CLIP-based discriminator, where $\mathcal{L}_{total} = \mathcal{L}_{rec} + \mathcal{L}_{per} + \lambda_{adv}\mathcal{L}_{adv}$.

As shown in Table IV, our experimental results demonstrate the effectiveness of incorporating text information in enhancing model performance. Comparisons across different configurations reveal notable improvements in both image detail recovery and semantic consistency. These results suggest that our proposed text-image fusion block (TIFBlock) and iterative enhancement module effectively align textual and visual features, providing crucial semantic guidance for generating high-resolution images that are both semantically consistent and realistic.

E. Analysis of the capability of LR-to-SR

To assess the text-to-image SR capabilities of our method, we perform comparative experiments against state-of-the-art models. As shown in Figure 7, we compare our approach with two leading conditional generation models, Stable Diffusion [54] and ControlNet [56], both of which leverage low-resolution 32×32 images in conjunction with their corresponding textual descriptions. As evidenced by the results, these models introduce several unwanted modifications in the generated images, deviating from the original visual information. In contrast, our method consistently produces clearer, more detailed outputs. This superior performance highlights the robustness of our approach in maintaining both semantic integrity and fine-grained pixel accuracy, emphasizing its advantages over competing methods in producing high-quality, text-aligned images.

F. Analysis of the editability in LR-to-SR transformation

To assess our model’s editability in low-to-high-resolution transformations, we select a subset of CUB test images for manipulation, as shown in Figure 8. In particular, Figure 8 (b) illustrates the bird’s color adjustments in the nape, crown,

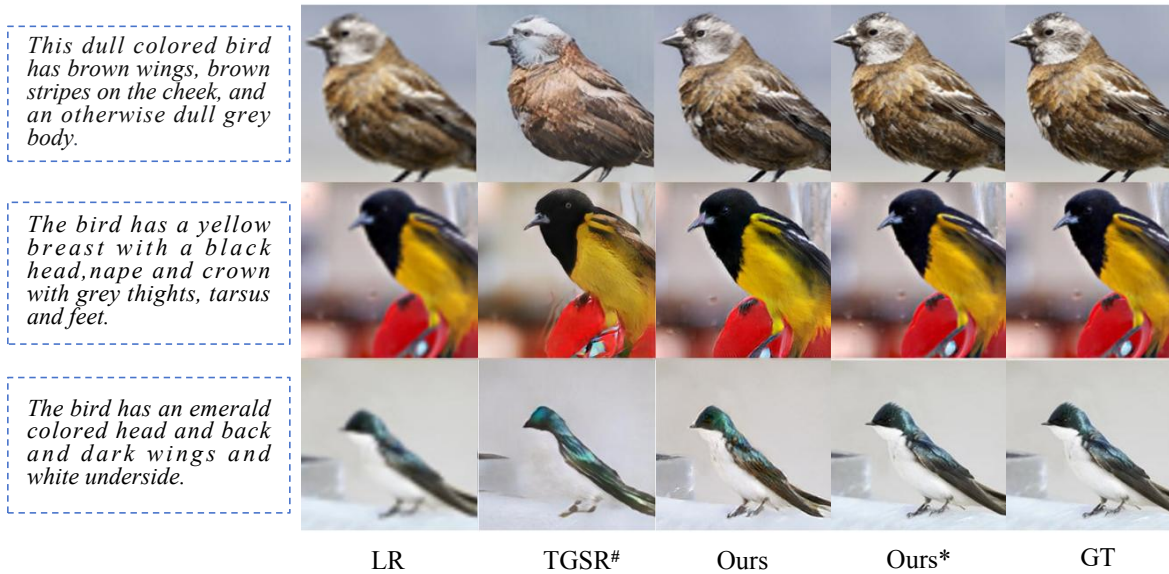


Fig. 4. Visual comparison with TGSR [17] our method. Notably, # indicates the results reported by the original paper. * represents the results of our method with the language-image pre-training model BLIP-2 and the text encoder BERT. The proposed method is compatible with various pre-trained multi-modality models. (Zoom in for the best view)



Fig. 5. Visual comparison of 4× SR results with two SOTA face SR methods, *i.e.*, DICGAN [18] and SuperFAN [9], and our method on the CelebA dataset.

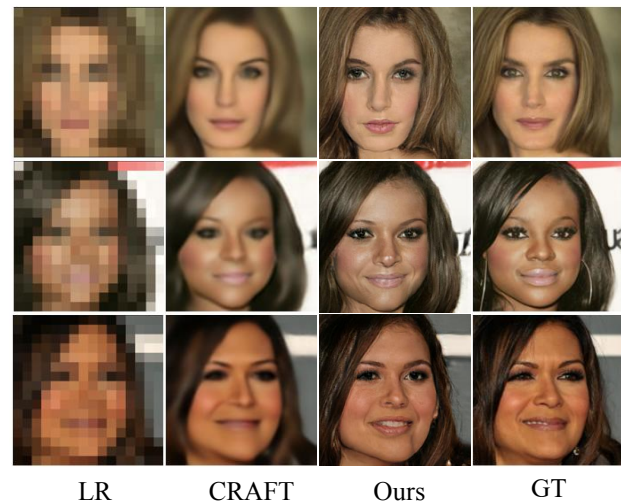


Fig. 6. Visual comparison of 16× SR results with CRAFT [19] and our method on the CelebA dataset.

and abdomen regions. Given the limitations of low-resolution inputs, the network emphasizes pixel-level accuracy over high-level semantic details, as evidenced by the slightly blurred black region around the bird’s head. Despite these constraints, our method successfully modifies the wing color in the abdomen area. When given the text prompt “yellow,” as shown in Figure 8 (c), the network effectively alters the wing color, with resulting hues varying across outputs.

G. Analysis of the effectiveness of multi-modal fusion and number of iteration layers

To evaluate the effectiveness of our multi-modal fusion module and the impact of different numbers of iterative fusion layers, we analyze heatmap outputs across layers within the multi-modal fusion module. As shown in Figure 9, each text

input is paired with a corresponding low-resolution image. Figure 9 (a) illustrates the output from the initial text fusion layer, where the network begins by generating an image loosely aligned with the bird. In subsequent layers, attention refines progressively: in Figure 9 (b), focus shifts to the bird’s neck and body, while further iterations in Figures 9 (c) and (d) progressively enhance finer details, including the bird’s feet and tarsus. These findings empirically confirm the effectiveness of our iterative refinement module, demonstrating that four iterations are sufficient to achieve high-quality, semantically consistent text-to-image super-resolution results.

H. Limitation

Despite the proposed method demonstrating superiority in the text-to-image super-resolution task, certain limitations

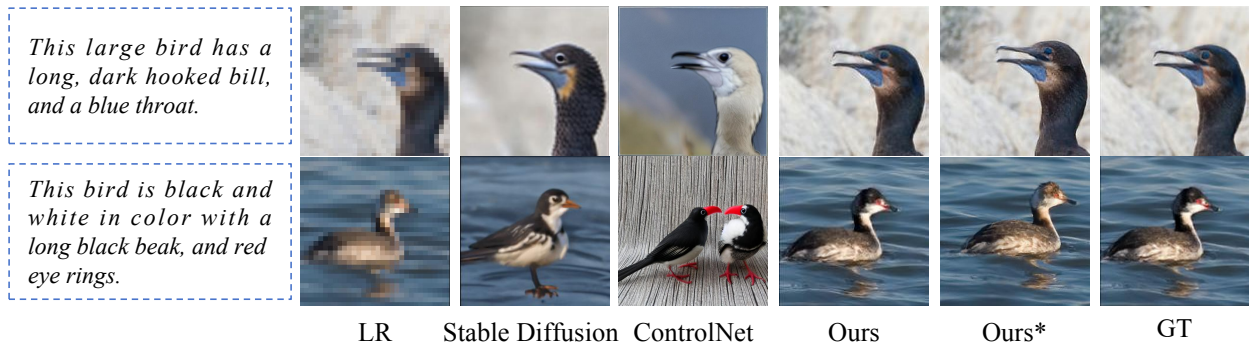


Fig. 7. Visual comparison of text-to-image SR task. We test the network with even lower-resolution images, sized at 32×32 . From the images, it can be observed that Stable Diffusion [54], and ControlNet [56] are no longer able to maintain consistency with the low-resolution images.

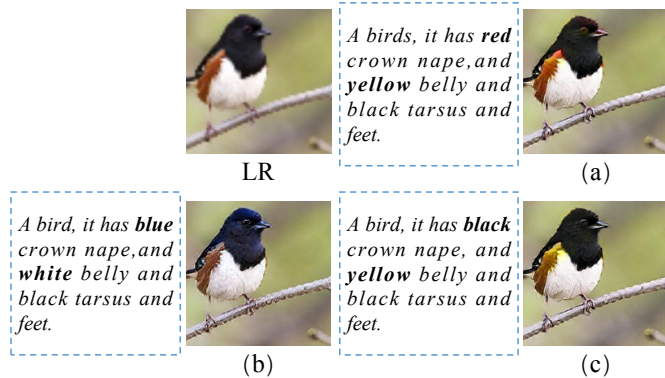


Fig. 8. Visualization of the results generated by our method under different text prompts. Our method demonstrates the capability to generate diverse and semantically consistent results.

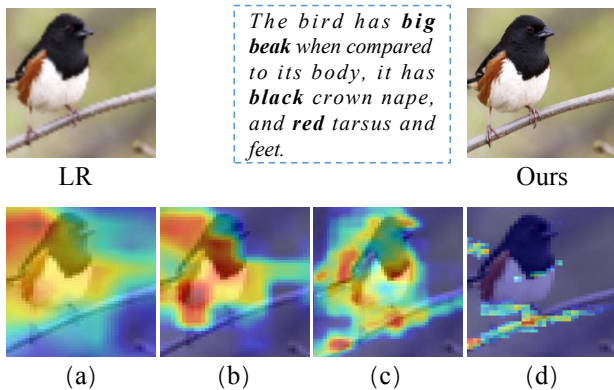


Fig. 9. Visualization of the heatmaps of low-resolution images during the super-resolution process. Subfigures (a), (b), (c), and (d) correspond to the results of text fusion at the first, second, third, and fourth layers, respectively, within the iterative refinement module

warrant consideration for future research. The CLIP-ViT-B/32 model effectively leverages textual information to enhance image quality, particularly in the realm of semantic-guided super-resolution. It effectively bridges the gap between textual and visual data, enabling precise control over the generation of high-resolution images. However, despite these strengths, the model can occasionally misinterpret ambiguous descriptions. For instance, as illustrated in Figure 10 (a), when instructed to generate an image featuring a "crown" on a bird, the model

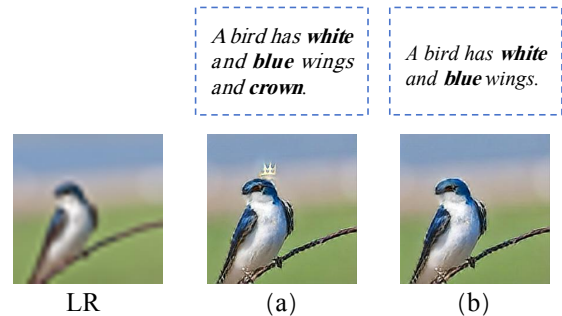


Fig. 10. Visualization of the results generated by our method under different text prompts. Given a low-resolution input image (a), our method produces super-resolution images guided by two distinct text descriptions: (b) and (c). While our method demonstrates impressive results, certain details in the generated images may exhibit deviations due to the inherent ambiguity of natural language semantics.

may incorrectly interpret the "crown" as a royal crown rather than the bird's crest. This misinterpretation underscores the necessity of precise language in prompts. As demonstrated in Figure 10 (b), removing the term "crown" and providing more specific context often yields the desired image. Future research could focus on enhancing the model's ability to disambiguate homonyms and develop a deeper understanding of context-specific semantics.

V. CONCLUSION

In this paper, we propose a novel multi-modal semantic consistency approach for large-factor image super-resolution (SR). Our method is capable of generating semantically consistent and visually realistic high-resolution images from significantly degraded low-resolution inputs. At the core of our approach is the Text-Image Fusion block (TIFBlock), which is strategically integrated with a pre-trained cross-modal model to form an iterative multi-modal collaborative fusion architecture. This framework enables the progressive recovery of image details while enhancing local semantic information. Comprehensive comparative experiments and ablation studies validate the efficacy of our SR method, demonstrating notable improvements in both the quality and realism of the generated high-resolution images. However, despite these advancements, our approach encounters certain challenges when processing

ambiguous textual descriptions, which can compromise the precision of the generated images. In future research, we aim to address this limitation by identifying and filtering out ambiguous terms before the text input model processes them. This refinement will ensure the model receives unambiguous instructions, enhancing the generated outputs' overall quality and consistency.

REFERENCES

- [1] B. Lim, S. Son, H. Kim, S. Nah, and K. Mu Lee, "Enhanced deep residual networks for single image super-resolution," in *Proceedings of the IEEE/CVF Conference on Computer Vision and Pattern Recognition workshops*, 2017, pp. 136–144. [1](#), [6](#), [7](#)
- [2] X. Wang, K. Yu, S. Wu, J. Gu, Y. Liu, C. Dong, Y. Qiao, and C. Change Loy, "Esrgan: Enhanced super-resolution generative adversarial networks," in *Proceedings of the European conference on computer vision workshops*, 2018, pp. 0–0. [1](#), [6](#), [7](#)
- [3] C. Tian, Y. Xu, W. Zuo, B. Zhang, L. Fei, and C.-W. Lin, "Coarse-to-fine cnn for image super-resolution," *IEEE Transactions on Multimedia*, vol. 23, pp. 1489–1502, 2020. [1](#)
- [4] C. Dong, C. C. Loy, K. He, and X. Tang, "Image super-resolution using deep convolutional networks," *Advances in Neural Information Processing Systems*, vol. 38, no. 2, pp. 295–307, 2015. [1](#), [2](#)
- [5] Y. Zhang, X. Yu, X. Lu, and P. Liu, "Pro-uigan: Progressive face hallucination from occluded thumbnails," *IEEE Transactions on Image Processing*, vol. 31, pp. 3236–3250, 2022. [1](#)
- [6] Y. Zhang, I. W. Tsang, J. Li, P. Liu, X. Lu, and X. Yu, "Face hallucination with finishing touches," *IEEE Transactions on Image Processing*, vol. 30, pp. 1728–1743, 2021. [1](#)
- [7] Y. Chen, Y. Tai, X. Liu, C. Shen, and J. Yang, "Fsnet: End-to-end learning face super-resolution with facial priors," in *Proceedings of the IEEE/CVF Conference on Computer Vision and Pattern Recognition*, 2018, pp. 2492–2501. [1](#), [2](#)
- [8] Z. Shen, W.-S. Lai, T. Xu, J. Kautz, and M.-H. Yang, "Deep semantic face deblurring," in *Proceedings of the IEEE/CVF Conference on Computer Vision and Pattern Recognition*, 2018, pp. 8260–8269. [1](#), [2](#)
- [9] A. Bulat and G. Tzimiropoulos, "Super-fan: Integrated facial landmark localization and super-resolution of real-world low resolution faces in arbitrary poses with gans," in *Proceedings of the IEEE/CVF Conference on Computer Vision and Pattern Recognition*, 2018, pp. 109–117. [1](#), [6](#), [7](#), [8](#)
- [10] J. Guo, X. Zhu, C. Zhao, D. Cao, Z. Lei, and S. Z. Li, "Learning meta face recognition in unseen domains," in *Proceedings of the IEEE/CVF Conference on Computer Vision and Pattern Recognition*, 2020, pp. 6163–6172. [1](#)
- [11] M. C. Buhler, A. Romero, and R. Timofte, "Deepsee: Deep disentangled semantic explorative extreme super-resolution," in *Proceedings of the Asian Conference on Computer Vision*, 2020. [1](#), [2](#)
- [12] C. Ma, Y. Rao, Y. Cheng, C. Chen, J. Lu, and J. Zhou, "Structure-preserving super resolution with gradient guidance," in *Proceedings of the IEEE/CVF Conference on Computer Vision and Pattern Recognition*, 2020, pp. 7769–7778. [1](#), [6](#), [7](#)
- [13] W. Li, J. Li, G. Gao, W. Deng, J. Zhou, J. Yang, and G.-J. Qi, "Cross-receptive focused inference network for lightweight image super-resolution," *IEEE Transactions on Multimedia*, vol. 26, pp. 864–877, 2023. [1](#)
- [14] Y. Zhao, Q. Teng, H. Chen, S. Zhang, X. He, Y. Li, and R. E. Sheriff, "Activating more information in arbitrary-scale image super-resolution," *IEEE Transactions on Multimedia*, 2024. [1](#)
- [15] D. Liu, X. Wang, R. Han, N. Bai, J. Hou, and S. Pang, "Cte-net: Contextual texture enhancement network for image super-resolution," *IEEE Transactions on Multimedia*, 2024. [1](#)
- [16] X. Wang, K. Yu, C. Dong, and C. C. Loy, "Recovering realistic texture in image super-resolution by deep spatial feature transform," in *Proceedings of the IEEE/CVF Conference on Computer Vision and Pattern Recognition*, 2018, pp. 606–615. [1](#)
- [17] C. Ma, B. Yan, Q. Lin, W. Tan, and S. Chen, "Rethinking super-resolution as text-guided details generation," in *Proceedings of the 30th ACM International Conference on Multimedia*, 2022, pp. 3461–3469. [1](#), [2](#), [6](#), [7](#), [8](#)
- [18] C. Ma, Z. Jiang, Y. Rao, J. Lu, and J. Zhou, "Deep face super-resolution with iterative collaboration between attentive recovery and landmark estimation," in *Proceedings of the IEEE/CVF Conference on Computer Vision and Pattern Recognition*, 2020, pp. 5569–5578. [2](#), [6](#), [7](#), [8](#)
- [19] A. Li, L. Zhang, Y. Liu, and C. Zhu, "Feature modulation transformer: Cross-refinement of global representation via high-frequency prior for image super-resolution," in *Proceedings of the IEEE/CVF International Conference on Computer Vision*, 2023, pp. 12 514–12 524. [2](#), [7](#), [8](#)
- [20] M. Jia, L. Tang, B.-C. Chen, C. Cardie, S. Belongie, B. Hariharan, and S.-N. Lim, "Visual prompt tuning," in *Proceedings of the European Conference on Computer Vision*, 2022. [1](#), [4](#)
- [21] M. Tao, B.-K. Bao, H. Tang, and C. Xu, "Galip: Generative adversarial clips for text-to-image synthesis," in *Proceedings of the IEEE/CVF Conference on Computer Vision and Pattern Recognition*, 2023, pp. 14 214–14 223. [1](#), [3](#), [4](#), [5](#), [6](#)
- [22] A. Radford, J. W. Kim, C. Hallacy, A. Ramesh, G. Goh, S. Agarwal, G. Sastry, A. Askell, P. Mishkin, J. Clark *et al.*, "Learning transferable visual models from natural language supervision," in *International Conference on Machine Learning*. PMLR, 2021, pp. 8748–8763. [2](#), [3](#), [4](#), [5](#)
- [23] W. Yang, X. Zhang, Y. Tian, W. Wang, J.-H. Xue, and Q. Liao, "Deep learning for single image super-resolution: A brief review," *IEEE Transactions on Multimedia*, vol. 21, no. 12, pp. 3106–3121, 2019. [2](#)
- [24] J. Kim, J. K. Lee, and K. M. Lee, "Accurate image super-resolution using very deep convolutional networks," in *Proceedings of the IEEE/CVF Conference on Computer Vision and Pattern Recognition*, 2016, pp. 1646–1654. [2](#)
- [25] Kim, Jiwon and Lee, Jung Kwon and Lee, Kyoung Mu, "Deeply-recursive convolutional network for image super-resolution," in *Proceedings of the IEEE/CVF Conference on Computer Vision and Pattern Recognition*, 2016, pp. 1637–1645. [2](#)
- [26] W. Shi, J. Caballero, F. Huszr, J. Totz, A. P. Aitken, R. Bishop, D. Rueckert, and Z. Wang, "Real-time single image and video super-resolution using an efficient sub-pixel convolutional neural network," in *Proceedings of the IEEE/CVF Conference on Computer Vision and Pattern Recognition*, 2016, pp. 1874–1883. [2](#)
- [27] C. Ledig, L. Theis, F. Huszr, J. Caballero, A. Cunningham, A. Acosta, A. Aitken, A. Tejani, J. Totz, Z. Wang *et al.*, "Photo-realistic single image super-resolution using a generative adversarial network," in *Proceedings of the IEEE/CVF Conference on Computer Vision and Pattern Recognition*, 2017, pp. 4681–4690. [2](#)
- [28] Y. Zhang, K. Li, K. Li, L. Wang, B. Zhong, and Y. Fu, "Image super-resolution using very deep residual channel attention networks," in *Proceedings of the European Conference on Computer Vision*, 2018, pp. 286–301. [2](#)
- [29] H. Zheng, M. Ji, H. Wang, Y. Liu, and L. Fang, "Crossnet: An end-to-end reference-based super resolution network using cross-scale warping," in *Proceedings of the European Conference on Computer Vision*, 2018, pp. 88–104. [2](#)
- [30] Z. Zhang, Z. Wang, Z. Lin, and H. Qi, "Image super-resolution by neural texture transfer," in *Proceedings of the IEEE/CVF Conference on Computer Vision and Pattern Recognition*, 2019, pp. 7982–7991. [2](#)
- [31] F. Yang, H. Yang, J. Fu, H. Lu, and B. Guo, "Learning texture transformer network for image super-resolution," in *Proceedings of the IEEE/CVF Conference on Computer Vision and Pattern Recognition*, 2020, pp. 5791–5800. [2](#)
- [32] Y. Jiang, K. C. Chan, X. Wang, C. C. Loy, and Z. Liu, "Robust reference-based super-resolution via c2-matching," in *Proceedings of the IEEE/CVF Conference on Computer Vision and Pattern Recognition*, 2021, pp. 2103–2112. [2](#)
- [33] X. Zhang, Z. Zheng, D. Gao, B. Zhang, Y. Yang, and T.-S. Chua, "Multi-view consistent generative adversarial networks for compositional 3d-aware image synthesis," *International Journal of Computer Vision*, vol. 131, no. 8, pp. 2219–2242, 2023. [2](#)
- [34] K. C. Chan, X. Wang, X. Xu, J. Gu, and C. C. Loy, "Glean: Generative latent bank for large-factor image super-resolution," in *Proceedings of the IEEE/CVF Conference on Computer Vision and Pattern Recognition*, 2021, pp. 14 245–14 254. [2](#)
- [35] X. Pan, X. Zhan, B. Dai, D. Lin, C. C. Loy, and P. Luo, "Exploiting deep generative prior for versatile image restoration and manipulation," *IEEE Transactions on Pattern Analysis and Machine Intelligence*, vol. 44, no. 11, pp. 7474–7489, 2021. [2](#)
- [36] X. Wang, Y. Li, H. Zhang, and Y. Shan, "Towards real-world blind face restoration with generative facial prior," in *Proceedings of the IEEE/CVF Conference on Computer Vision and Pattern Recognition*, 2021, pp. 9168–9178. [2](#)

- [37] T. Yang, P. Ren, X. Xie, and L. Zhang, "Gan prior embedded network for blind face restoration in the wild," in *Proceedings of the IEEE/CVF Conference on Computer Vision and Pattern Recognition*, 2021, pp. 672–681. [2](#)
- [38] Y. Suo, Z. Zheng, X. Wang, B. Zhang, and Y. Yang, "Jointly harnessing prior structures and temporal consistency for sign language video generation," *ACM Transactions on Multimedia Computing, Communications and Applications*, vol. 20, no. 6, pp. 1–18, 2024. [3](#)
- [39] Z. Huang, Z. Zheng, C. Yan, H. Xie, Y. Sun, J. Wang, and J. Zhang, "Real-world automatic makeup via identity preservation makeup net," in *International Joint Conference on Artificial Intelligence*. International Joint Conference on Artificial Intelligence, 2021. [3](#)
- [40] B. Li, X. Qi, P. Torr, and T. Lukasiewicz, "Lightweight generative adversarial networks for text-guided image manipulation," *Advances in Neural Information Processing Systems*, vol. 33, pp. 22 020–22 031, 2020. [3](#)
- [41] H. Zhang, T. Xu, H. Li, S. Zhang, X. Wang, X. Huang, and D. N. Metaxas, "Stackgan: Text to photo-realistic image synthesis with stacked generative adversarial networks," in *Proceedings of the IEEE/CVF International Conference on Computer Vision*, 2017, pp. 5907–5915. [3](#)
- [42] T. Xu, P. Zhang, Q. Huang, H. Zhang, Z. Gan, X. Huang, and X. He, "AttnGAN: Fine-grained text to image generation with attentional generative adversarial networks," in *Proceedings of the IEEE/CVF Conference on Computer Vision and Pattern Recognition*, 2018, pp. 1316–1324. [3](#)
- [43] M. Zhu, P. Pan, W. Chen, and Y. Yang, "Dm-gan: Dynamic memory generative adversarial networks for text-to-image synthesis," in *Proceedings of the IEEE/CVF Conference on Computer Vision and Pattern Recognition*, 2019, pp. 5802–5810. [3](#)
- [44] M. Tao, H. Tang, F. Wu, X.-Y. Jing, B.-K. Bao, and C. Xu, "Df-gan: A simple and effective baseline for text-to-image synthesis," in *Proceedings of the IEEE/CVF Conference on Computer Vision and Pattern Recognition*, 2022, pp. 16 515–16 525. [3](#), [5](#)
- [45] Y. Zhou, R. Zhang, C. Chen, C. Li, C. Tensmeyer, T. Yu, J. Gu, J. Xu, and T. Sun, "Towards language-free training for text-to-image generation," in *Proceedings of the IEEE/CVF Conference on Computer Vision and Pattern Recognition*, 2022, pp. 17 907–17 917. [3](#)
- [46] G. Kwon and J. C. Ye, "Clipstyler: Image style transfer with a single text condition," in *Proceedings of the IEEE/CVF Conference on Computer Vision and Pattern Recognition*, 2022, pp. 18 062–18 071. [3](#)
- [47] T.-J. Fu, X. E. Wang, and W. Y. Wang, "Language-driven artistic style transfer," in *Proceedings of the European Conference on Computer Vision*. Springer, 2022, pp. 717–734. [3](#)
- [48] H. Dong, S. Yu, C. Wu, and Y. Guo, "Semantic image synthesis via adversarial learning," in *Proceedings of the IEEE/CVF International Conference on Computer Vision*, 2017, pp. 5706–5714. [3](#)
- [49] B. Li, X. Qi, T. Lukasiewicz, and P. H. Torr, "Manigan: Text-guided image manipulation," in *Proceedings of the IEEE/CVF Conference on Computer Vision and Pattern Recognition*, 2020, pp. 7880–7889. [3](#)
- [50] J. Wang, G. Lu, H. Xu, Z. Li, C. Xu, and Y. Fu, "Manitrans: Entity-level text-guided image manipulation via token-wise semantic alignment and generation," in *Proceedings of the IEEE/CVF Conference on Computer Vision and Pattern Recognition*, 2022, pp. 10 707–10 717. [3](#)
- [51] L. Zeng, Z. Zheng, Y. Wei, and T.-s. Chua, "Instilling multi-round thinking to text-guided image generation," *arXiv preprint arXiv:2401.08472*, 2024. [3](#)
- [52] J. Ho, C. Saharia, W. Chan, D. J. Fleet, M. Norouzi, and T. Salimans, "Cascaded diffusion models for high fidelity image generation," *Journal of Machine Learning Research*, vol. 23, no. 47, pp. 1–33, 2022. [3](#)
- [53] A. Van Den Oord, O. Vinyals *et al.*, "Neural discrete representation learning," *Advances in Neural Information Processing Systems*, vol. 30, 2017. [3](#)
- [54] R. Rombach, A. Blattmann, D. Lorenz, P. Esser, and B. Ommer, "High-resolution image synthesis with latent diffusion models," in *Proceedings of the IEEE/CVF Conference on Computer Vision and Pattern Recognition*, 2022, pp. 10 684–10 695. [3](#), [7](#), [9](#)
- [55] A. Nichol, P. Dhariwal, A. Ramesh, P. Shyam, P. Mishkin, B. McGrew, I. Sutskever, and M. Chen, "Glide: Towards photorealistic image generation and editing with text-guided diffusion models," *arXiv preprint arXiv:2112.10741*, 2021. [3](#)
- [56] L. Zhang, A. Rao, and M. Agrawala, "Adding conditional control to text-to-image diffusion models," in *Proceedings of the IEEE/CVF International Conference on Computer Vision*, 2023, pp. 3836–3847. [3](#), [7](#), [9](#)
- [57] C. Saharia, W. Chan, S. Saxena, L. Li, J. Whang, E. L. Denton, K. Ghasemipour, R. Gontijo Lopes, B. Karagol Ayan, T. Salimans *et al.*, "Photorealistic text-to-image diffusion models with deep language understanding," *Advances in Neural Information Processing Systems*, vol. 35, pp. 36 479–36 494, 2022. [3](#)
- [58] E. J. Hu, Y. Shen, P. Wallis, Z. Allen-Zhu, Y. Li, S. Wang, L. Wang, and W. Chen, "Lora: Low-rank adaptation of large language models," *arXiv preprint arXiv:2106.09685*, 2021. [3](#)
- [59] C. Mou, X. Wang, L. Xie, Y. Wu, J. Zhang, Z. Qi, and Y. Shan, "T2i-adapter: Learning adapters to dig out more controllable ability for text-to-image diffusion models," in *Proceedings of the AAAI Conference on Artificial Intelligence*, vol. 38, no. 5, 2024, pp. 4296–4304. [3](#)
- [60] Z. Yue, J. Wang, and C. C. Loy, "Resshift: Efficient diffusion model for image super-resolution by residual shifting," *Advances in Neural Information Processing Systems*, vol. 36, 2024. [3](#)
- [61] J. Wang, P. Liu, J. Liu, and W. Xu, "Text-guided eyeglasses manipulation with spatial constraints," *IEEE Transactions on Multimedia*, vol. 26, pp. 4375–4388, 2024. [3](#)
- [62] S. Yang, Y. Zhou, Z. Zheng, Y. Wang, L. Zhu, and Y. Wu, "Towards unified text-based person retrieval: A large-scale multi-attribute and language search benchmark," in *Proceedings of the 31st ACM International Conference on Multimedia*, 2023, pp. 4492–4501. [3](#)
- [63] S. Reed, Z. Akata, X. Yan, L. Logeswaran, B. Schiele, and H. Lee, "Generative adversarial text to image synthesis," in *International Conference on Machine Learning*. PMLR, 2016, pp. 1060–1069. [3](#)
- [64] J. Johnson, A. Alahi, and L. Fei-Fei, "Perceptual losses for real-time style transfer and super-resolution," in *Proceedings of the European Conference on Computer Vision*. Springer, 2016, pp. 694–711. [5](#)
- [65] K. Simonyan and A. Zisserman, "Very deep convolutional networks for large-scale image recognition," in *International Conference on Learning Representations*, 2015. [6](#)
- [66] T.-Y. Lin, M. Maire, S. Belongie, J. Hays, P. Perona, D. Ramanan, P. Dollr, and C. L. Zitnick, "Microsoft coco: Common objects in context," in *Proceedings of the European Conference on Computer Vision*. Springer, 2014, pp. 740–755. [6](#)
- [67] C. Wah, S. Branson, P. Welinder, P. Perona, and S. Belongie, "The caltech-ucsd birds-200-2011 dataset," California Institute of Technology, Tech. Rep. CNS-TR-2011-001, 2011. [6](#)
- [68] D. Cheng, B. Price, S. Cohen, and M. S. Brown, "Beyond white: Ground truth colors for color constancy correction," in *Proceedings of the IEEE/CVF International Conference on Computer Vision*, 2015, pp. 298–306. [6](#)
- [69] Z. Wang, "Image quality assessment: Form error visibility to structural similarity," *IEEE Trans. Image Process.*, vol. 13, no. 4, pp. 604–606, 2004. [6](#)
- [70] Y. Blau, R. Mechrez, R. Timofte, T. Michaeli, and L. Zelnik-Manor, "The 2018 pirm challenge on perceptual image super-resolution," in *Proceedings of the European Conference on Computer Vision workshops*, 2018, pp. 334–355. [6](#)
- [71] J. Li, D. Li, S. Savarese, and S. Hoi, "Blip-2: Bootstrapping language-image pre-training with frozen image encoders and large language models," in *International Conference on Machine Learning*. PMLR, 2023, pp. 19 730–19 742. [6](#)
- [72] J. Devlin, M.-W. Chang, K. Lee, and K. Toutanova, "Bert: Pre-training of deep bidirectional transformers for language understanding," in *Proceedings of the 2019 Conference of the North American Chapter of the Association for Computational Linguistics: Human Language Technologies*, 2018. [7](#)